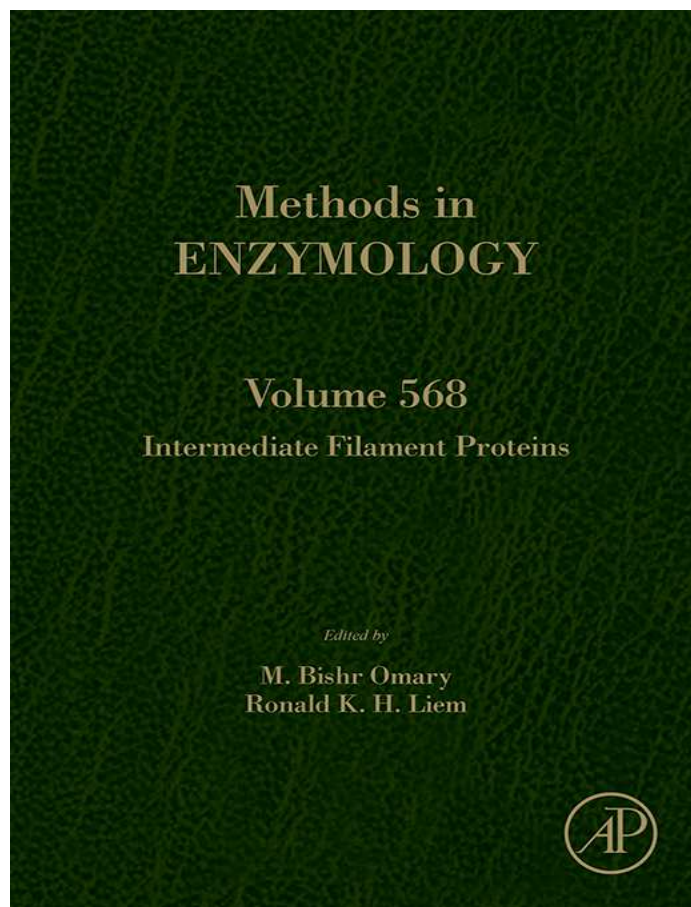


**Provided for non-commercial research and educational use only.
Not for reproduction, distribution or commercial use.**

This chapter was originally published in the book *Methods in Enzymology*, Vol. 568 published by Elsevier, and the attached copy is provided by Elsevier for the author's benefit and for the benefit of the author's institution, for non-commercial research and educational use including without limitation use in instruction at your institution, sending it to specific colleagues who know you, and providing a copy to your institution's administrator.



All other uses, reproduction and distribution, including without limitation commercial reprints, selling or licensing copies or access, or posting on open internet sites, your personal or institution's website or repository, are prohibited. For exceptions, permission may be sought for such use through Elsevier's permissions site at:

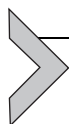
<http://www.elsevier.com/locate/permissionusematerial>

From Nicole Schwarz, Marcin Moch, Reinhard Windoffer and Rudolf E. Leube, Multidimensional Monitoring of Keratin Intermediate Filaments in Cultured Cells and Tissues. In: M. Bishr Omary and Ronald K.H. Liem, editors, *Methods in Enzymology*, Vol. 568, Burlington: Academic Press, 2016, pp. 59-83.

ISBN: 978-0-12-803470-5

© Copyright 2016 Elsevier Inc.

Academic Press



Multidimensional Monitoring of Keratin Intermediate Filaments in Cultured Cells and Tissues

Nicole Schwarz¹, Marcin Moch¹, Reinhard Windoffer, Rudolf E. Leube²

Institute of Molecular and Cellular Anatomy, RWTH Aachen University, Aachen, Germany

²Corresponding author: e-mail address: rleube@ukaachen.de

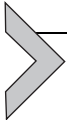
Contents

1. Introduction	60
2. 3D Imaging of Keratin Intermediate Filaments in Cultured Cells	62
2.1 Microscopes	64
2.2 Preparation of Imaging Medium	65
2.3 Surface Coating	65
2.4 Preparation of Cells for Imaging	66
2.5 Image Acquisition	67
2.6 Keratin Network Normalization	67
2.7 Measuring Keratin Movement	68
2.8 Keratin Bulk Flow Analysis	70
2.9 Keratin Turnover Measured by FRAP	72
3. 3D Imaging of Keratin Intermediate Filaments in Murine Preimplantation Embryos	75
3.1 Embryo Collection and Cultivation	75
3.2 Imaging of Preimplantation Embryos	76
3.3 Image Processing and Analysis	78
4. Outlook	80
Acknowledgments	81
References	81

Abstract

Keratin filaments are a hallmark of epithelial differentiation. Their cell type-specific spatial organization and dynamic properties reflect and support epithelial function. To study this interdependency, imaging of fluorescently tagged keratins is a widely used method by which the temporospatial organization and behavior of the keratin intermediate filament network can be analyzed in living cells. Here, we describe methods that have been adapted and optimized to dissect and quantify keratin intermediate filament network dynamics in vital cultured cells and functional tissues.

¹ These authors contributed equally to this work.



1. INTRODUCTION

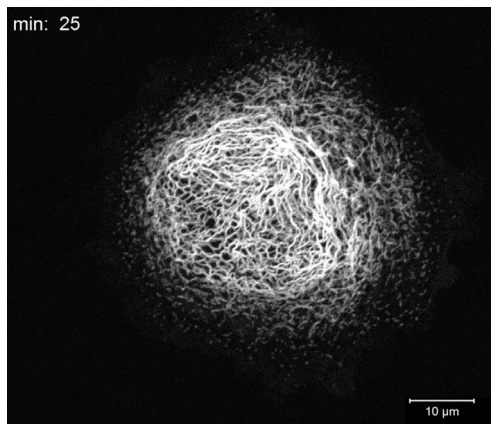
The intermediate filament network is a complex three-dimensional (3D) scaffold in metazoan cells contributing for the most part to the mechanical stability of cells and was therefore originally considered static in nature. This view was abandoned when different stimuli were found to induce profound organizational changes. During mitosis, for example, keratin intermediate filament networks are rapidly disassembled and appear as aggregates, followed by their reassembly in daughter cells (Franke, Schmid, Grund, & Geiger, 1982; Lane, Goodman, & Trejdosiewicz, 1982). The precise sequel of changes in the organization of the intermediate filament cytoskeleton, however, was difficult to deduce from still images. Subsequently, methods became available, which allowed monitoring of intermediate filaments in living cells.

Early approaches were based on the injection of fluorescently tagged proteins and antibodies (Mittal, Sanger, & Sanger, 1989; Okabe, Miyasaka, & Hirokawa, 1993; Vikstrom, Lim, Goldman, & Borisy, 1992), which revealed details of network reorganization during mitosis and aspects of filament turnover during interphase. Major problems in these studies were the precise regulation of expression and rapid photobleaching, which prevented long-term live cell imaging.

With the introduction of green fluorescent protein (GFP) as a marker for expression in 1994 (Chalfie, Tu, Euskirchen, Ward, & Prasher, 1994) and subsequent usage as a protein tag (Cubitt et al., 1995), imaging of protein distribution in living cells has been revolutionized. Initial studies on GFP-vimentin revealed an intrinsically dynamic and shape-changing network (Ho, Martys, Mikhailov, Gundersen, & Liem, 1998; Yoon, Moir, Prahlad, & Goldman, 1998). During spreading and adhesion of cells, three structural forms of intermediate filaments were distinguished: motile small particles, short nonconnected filamentous structures referred to as squiggles, and long intermediate filaments organized in a network (Prahlad, Yoon, Moir, Vale, & Goldman, 1998). It was proposed that the particles give rise to squiggles, which are incorporated into longer filaments (Prahlad et al., 1998). In neuronal cells, rapidly moving particles were identified by live cell imaging of GFP-tagged neurofilaments which intercalate into neurofilament bundles (Wang, Ho, Sun, Liem, & Brown, 2000; Yuan et al., 2009). Interestingly, short filaments termed keratin precursors were identified in the periphery of keratin-containing epithelial cells (Windoffer & Leube, 1999).

In case of the keratin intermediate filaments, a turnover cycle was proposed based on time-lapse fluorescence imaging, fluorescence recovery after photobleaching (FRAP) experiments, and photoactivation studies (Kölsch, Windoffer, Würflinger, Aach, Leube, 2010; Leube, Moch, Kölsch, & Windoffer, 2011; Windoffer, Beil, Magin, & Leube, 2011; Windoffer, Wöll, Strnad, & Leube, 2004; Yoon et al., 2001). Thus, keratin filament precursors nucleate in the cell periphery and constantly move inward, while they elongate and integrate into the peripheral keratin network. The network either matures into a stable nuclear cage or disassembles into soluble and highly diffusible subunits. These soluble subunits are reutilized in the cell periphery for another cycle of assembly and disassembly. [Movie 1](#) (<http://dx.doi.org/10.1016/bs.mie.2015.07.034>) and corresponding [Fig. 1](#) highlight features of the keratin cycle.

The studies made so far face two major challenges. On one hand, the subtle and physiologically most relevant alterations in keratin dynamics are often missed and/or difficult to measure (Baribault, Blouin, Bourgon, & Marceau, 1989; Chung, Murray, Eyk, & Coulombe, 2012; Keski-Oja, Lehto, & Virtanen, 1981; Ku & Omary, 1997). To overcome this, we developed a method to quantitatively map keratin intermediate filament motility and turnover at subcellular resolution (Moch, Herberich, Aach, Leube, & Windoffer, 2013). On the other hand, the additional expression of the fluorescently tagged keratin filaments may perturb network dynamics and organization (Windoffer & Leube, 1999). To mimic



Movie 1 Time-lapse fluorescence recording of keratin 13-EGFP in AK13-pax1 cells (corresponding [Fig. 1](#)). Major steps of the keratin cycle, namely nucleation, elongation, integration, and bundling, are seen.

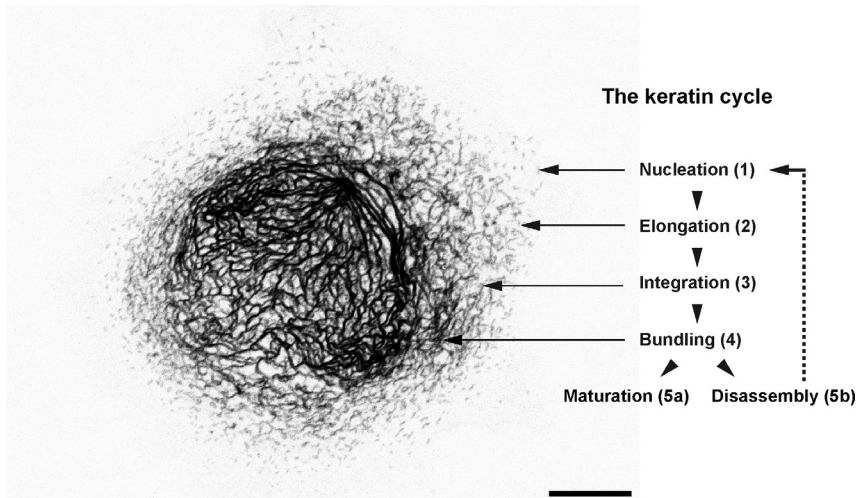
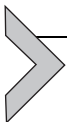


Figure 1 Keratin cycle of assembly and disassembly. The figure shows a representative still image of a time-lapse recording of keratin 13-EGFP fluorescence (inverse presentation) in vulvar carcinoma-derived AK13-pax1 cells (Leube, Moch, & Windoffer, 2015). Cells were plated on a laminin 332-rich matrix 20 h prior to confocal microscopy. The confocal plane shown represents the bottom part of the cell below the nucleus. On the right, the major steps of the keratin cycle, which can be best appreciated in [Movie 1](#), are denoted: nucleation of keratin particles in the cell periphery (1), elongation of these particles (2), subsequent integration of the inward-moving and growing particles into the peripheral network (3), bundling of inward-moving filaments (4), and either maturation into a stable perinuclear cage-like structure (5a) or disassembly into rapidly diffusible subunits (5b) that can be reutilized for another round of assembly and disassembly. Scale bar: 10 μm .

the wild-type situation as closely as possible, we generated a knock-in mouse model that produces fluorescently tagged keratin 8 instead of the endogenous keratin 8 (Schwarz, Windoffer, Magin, & Leube, 2015). This model allows the analysis of keratin dynamics in the physiological 3D context of the preimplantation embryo and facilitates the examination of *de novo* network formation.



2. 3D IMAGING OF KERATIN INTERMEDIATE FILAMENTS IN CULTURED CELLS

Imaging keratins in cells producing fluorescently tagged keratins has become routine in several laboratories (Berault et al., 2012; Fois et al., 2013; Liovic, Mogensen, Prescott, & Lane, 2003; Rolli, Seufferlein, Kemkemer, & Spatz, 2010; Windoffer & Leube, 1999; Yoon et al., 2001).

Conditions have been described to monitor keratin dynamics in 3D during the entire cell cycle (Windoffer & Leube, 2004). Examples are presented in Fig. 2 and corresponding Movie 2 (<http://dx.doi.org/10.1016/bs.mie.2015.07.034>). They show that the majority of the keratin network is located in the basal part of cultured cells adjacent to the extracellular matrix. It surrounds the nucleus in a cage-like structure and thins out toward the apical cytoplasm (Fig. 2A). Rapid breakdown of the network is detected at the onset of mitosis resulting in multiple granular aggregates, which are used for reassembly of the network in the daughter cells after completion of cell division (Windoffer & Leube, 2001, 2004). The sequence shown in Fig. 2B and Movie 2 demonstrates that the distribution of keratins can be monitored in 3D for long periods without disturbing cell viability and photobleaching. But keep in mind that scanning cells in three dimensions considerably increases cell stress by

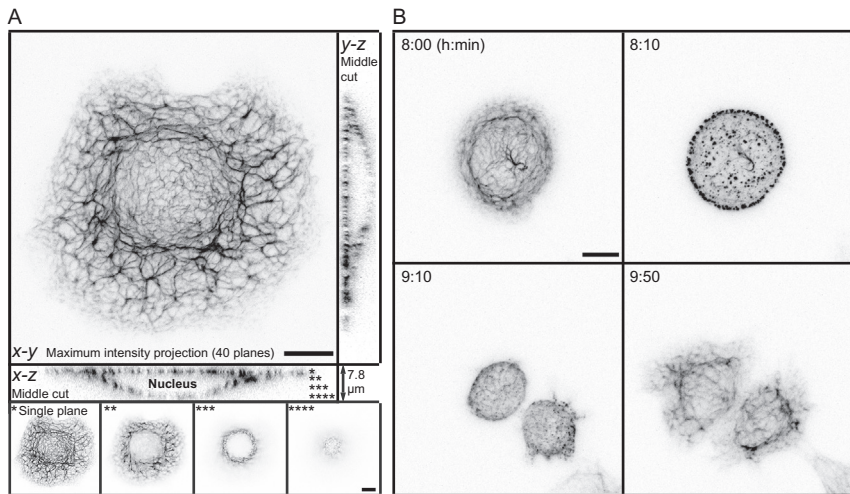
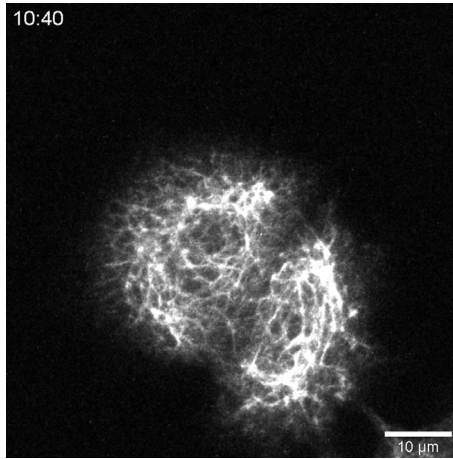


Figure 2 Keratin network morphology in interphase and during cell division. AK13-1 cells stably expressing keratin 13-EGFP were cultivated on a laminin 332-rich matrix without FCS for 48 h (A) and for 60 h (B). The fluorescence recorded by confocal laser scanning microscopy in the cell shown in (A) at high resolution depicts the arrangement of the keratin network during interphase as a maximum intensity projection of 40 planes and transverse sections on top and as single plane recordings at the bottom. The keratin network forms a cage around the nucleus and is mostly concentrated at the bottom plane of the cell (single star). The images in (B) are taken from Movie 2 that was recorded at lower spatial resolution (13 planes, 0.88 μm steps). In this instance, background was removed by Gaussian filtering using Fiji software. The inverse fluorescence micrographs show stages of keratin network disassembly before cell division and network reassembly thereafter. These processes occur within minutes and are independent of protein degradation and biosynthesis. Scale bars: 10 μm .



Movie 2 Maximum intensity projections of keratin 13-EGFP fluorescence detecting keratin network reorganization during cell division (corresponding Fig. 2B).

generating reactive oxygen species. The damage is not solely restricted to the imaged section but affects the entire cell. The stress is substantial when fluorescence is recorded repeatedly at high spatial resolution. Addition of antioxidants (e.g., 4 mM *N*-acetyl-L-cysteine; [Strnad, Windoffer, & Leube, 2003](#)) may alleviate the problem, although we never observed beneficial effects for the protocols presented here.

In the following sections, we will focus on new methodology to measure keratin dynamics in living cells under standardized conditions.

2.1 Microscopes

The methods described here were developed for a conventional confocal laser scanning microscope (LSM 710 Duo; Carl Zeiss). Excitation of EGFP or EYFP is performed at 488 nm using an Argon-ion laser (laser module LGK 7872 ML8). Images are acquired with a 63×1.4 N.A. Differential interference contrast (DIC) oil immersion objective. Focus drift in time series is corrected with the Definite Focus system (Carl Zeiss). The entire microscope is encased in a Plexiglas incubation chamber, and stable temperature is maintained with the help of a heating unit (Incubator XL LSM 710 S1). The complete microscope is mounted on a Vibration Isolated Workstation (Newport Corporation). Alternatively, other confocal laser scanning microscopes can be used. But it should be kept in mind that the keratin motion analysis software described below was not developed for charge-coupled device (CCD) cameras that are used, for example, in confocal spinning disc microscopy.

2.2 Preparation of Imaging Medium

For optimal fluorescence signal quality, experiments should be performed in cell culture medium without phenol red to avoid autofluorescence. If the microscope is not equipped with a CO₂ climate chamber, commercially available HEPES-buffered cell medium or self-made Hanks-HEPES imaging medium can be added prior to experiments. Be aware that several commercial media are often yellowish, which will increase in intensity upon addition of fetal calf serum (FCS). In our experience, however, this does not affect the signal quality of green and yellow fluorophores:

1. Prepare 500 ml Hanks-HEPES imaging medium by adding 50 ml Hanks' Balanced Salt Solution (HBSS, 10 ×; 14185052, Life Technologies), 5 ml nonessential amino acids (100 ×; 1114-035, Life Technologies), 10 ml essential amino acids (50 ×; 11130-036, Life Technologies), 5 ml GlutaMAX™ (35050-038, Life Technologies), 12.5 ml HEPES (1 M; 15630-056, Life Technologies), 5 ml *N*-acetyl-L-cysteine (0.48 M, freshly dissolved; A7250, Sigma-Aldrich), and 0.175 g sodium bicarbonate (HN01, Carl Roth).
2. Adjust volume to 500 ml using distilled H₂O (Aqua B. Braun).
3. Adjust pH to 7.4 using HCl.
4. Sterile filtrate through a 0.22-μm filter (Merck Millipore).
5. Store up to a month at 4 °C or for long-term at -20 °C.

2.3 Surface Coating

For optical imaging, cells are typically grown on glass. For cell adhesion and spreading, the glass surface should be coated with appropriate matrix proteins. The choice of matrix proteins affects cell shape and intracellular signaling. Ideally, single cells should be circular, flat, and stably attached. A number of commercial matrix proteins may fulfill these requirements. For the epithelial cell lines that we routinely use, we prefer a laminin 332-rich matrix preparation from 804G cells (Langhofer, Hopkinson, & Jones, 1993):

1. Grow rat bladder carcinoma-derived 804G cells in Dulbecco's Modified Eagle Medium (DMEM; D0819, Sigma-Aldrich) supplemented with 10% FCS (Life Technologies) to confluence in a glass bottom dish (35 mm Petri dish with 14 mm glass surface diameter and glass thickness no. 1.5; P35G-0.17-14-C, MatTek).
2. "Derroof" cells 1 day after reaching confluence by adding ice-cold 20 mM NH₄OH and incubating at room temperature for 10–15 min.

3. Discard NH_4OH and flush off remaining debris using distilled H_2O (Aqua B. Braun). This procedure will leave behind extracellular proteins on the glass surface.
4. Wash surface two times with distilled H_2O and two times with PBS (D8537, Sigma-Aldrich).
5. Remove PBS.
6. Coated vessels can be stored up to 2 months at $-20\text{ }^\circ\text{C}$.

2.4 Preparation of Cells for Imaging

It is important to carefully select the conditions for cell culture to achieve reproducible kinetics of spreading and adhesion as well as growth and cell densities at defined times after passaging. Even then, heterogeneity is still a major challenge in quantitative imaging of intracellular structures in single cells of clonal cell lines. Another concern is biochemical stress. We therefore cultivate our cells in the absence of antibiotics and selective drugs. For cell lines that are difficult to grow at low cell density, we recommend preconditioned culture medium. This medium is obtained from dense cell cultures and is enriched in secreted factors. It is mixed with fresh cell culture medium at ratios that are empirically determined:

1. Seed $\approx 25,000$ A431 cells in DMEM without FCS on glass bottom dishes coated with laminin 332-rich matrix (see Protocol 2.3).
2. Cells are typically kept in the incubator for 19–57 h prior to use.
3. Prewarm the microscope to $37\text{ }^\circ\text{C}$. Note that the objective will take longer until it is warm when it has no additional heating. It is advisable to test the temperature with a thermometer in a small water reservoir. Thorough adjustment and equilibration of the temperature is crucial for focal stability during image acquisition.
4. Prewarm Hanks-HEPES imaging medium (see Protocol 2.2) to $37\text{ }^\circ\text{C}$.
5. Remove cell culture medium from the glass bottom dish and add 1 ml Hanks-HEPES imaging medium.
6. Select suitable cells for time-lapse recording of fluorescence and phase contrast. Important criteria are that the selected cells are representative for all cells in a given culture dish and that most of the fluorescence signal is restricted to a single confocal plane. This is usually the case in extremely flat cells. For generation of topological maps of keratin dynamics, selected cells should have a similar size and a pancake-like circular shape with the nucleus in the cell center. Cells with more than one nucleus should be excluded from analysis.

2.5 Image Acquisition

The motion analysis method described here is optimized for confocal laser scanning microscopy where a photomultiplier tube (PMT) is used for signal detection. In comparison to images obtained with CCDs, such recordings provide a higher-than-average noise to signal ratio and eliminate efficiently out of focus signals. The slow laser scanning speed, which is in the range of several seconds per frame, is not problematic because keratins within the network move rather slowly. Of note, the motility of keratin precursors outside of the keratin network is not reliably measured by the method described here, because many of these rare particles (less than 1% of all keratins) are removed by the denoising during image analysis:

1. The scanning time per $67\ \mu\text{m} \times 67\ \mu\text{m}$ should be less than 30 s to avoid distortion of moving structures (22 s in the examples shown here).
2. The images should be acquired at a resolution of 1024×1024 pixel. The signal detection range should be 16 bit.
3. The signal should be detected in a single scan for best accuracy without averaging of multiple scans into one image. It is also recommended to use unidirectional scanning instead of faster bidirectional scanning because of possible misalignment of scanned lines.
4. A laser intensity should be selected with minimal bleaching of fluorophores. In general, the signal does not have to be very strong as long as the background is low. This aspect is also relevant for choosing the optimal detector gain.
5. The pinhole can be slightly opened to increase the amount of detected light (2 airy units are optimal). In this way, the thickness of the focal plane is increased and thereby allows a more complete detection of the keratin network.
6. It is essential that the focus remains stable during the entire imaging period. Since manual adjustment requires extreme patience and diligence, an automated focus stabilization system is highly recommended. Some older microscopes can be upgraded by the manufacturer with such a device.
7. Time series are routinely done at intervals of 30 s for 10–15 min.

2.6 Keratin Network Normalization

Cells that are analyzed for longer time periods often show cell shape changes, especially when treated with different modulators. These changes affect the keratin network morphology and result in keratin displacement that is not related to active keratin transport inside the cell. These anomalies can be

corrected in two different ways. When the changes occur only in a small part of the cell, it is possible to remove the regions from analysis by cutting them out or blackening. However, the faster and more elegant solution is to normalize the keratin network into a circular shape with a defined diameter. This can be done with the KeraMove software (http://www.moca.rwth-aachen.de/pubs/2013_01/softwarepackage_KeraMove_KeraDyn.zip). In this process, the border of the keratin network (which does not correspond to the cell border) is extended in every frame to the border of the predefined shape. This procedure sometimes induces errors but can help to analyze and compare data obtained from differently sized and shaped cells. The size of the newly produced networks is not related in a linear way to the data before transformation, but the keratin networks in these images can be tracked efficiently by the KeraMove software. This method is recommended for cells that show cell shape changes less than 10% of the total cell area as assessed by measuring the extension of the fluorescently tagged keratin network. It can yield almost perfectly symmetrical heat maps of keratin movement and bulk flow when results from many cells are overlaid:

1. Run the open source software KeraMove (http://www.moca.rwth-aachen.de/pubs/2013_01/softwarepackage_KeraMove_KeraDyn.zip).
2. Select “perform shape normalization.”

2.7 Measuring Keratin Movement

The motion of fluorescently tagged keratin networks from confocal time-lapse recordings can be detected with the open source software KeraMove (Moch et al., 2013). The software and a user manual are provided at http://www.moca.rwth-aachen.de/pubs/2013_01/softwarepackage_KeraMove_KeraDyn.zip:

1. Start KeraMove as described in the manual. Set “maximum sought displacement” to 1200 nm. The software generates maps of mean keratin movement per pixel from analyzed recordings (output file: mag-OfMeanMotion.raw). The speed is calculated at the level of single pixels from the registered filaments. Therefore, the displacement of every of these pixels is tracked independently of its direction as long as it occurs in the 2D plane of the cell bottom. If keratin network normalization is needed, proceed as described in [Section 2.6](#).
2. Import output file into Fiji software (freely available at <http://fiji.sc/Fiji>) as a heat map (submenu: File → import → raw; image type: 32 bit real,

little-endian byte order). The speed of movement is coded in 32-bit gray values in the same unit as in the analyzed recordings. The calculated speed corresponds to the sum of speed calculated for all frames divided by the number of frames. Do not forget that the speed has to be multiplied by the appropriate factor to obtain the speed per minute. For example, if images were acquired at 30 s intervals, the speed has to be multiplied by 2. Next, a threshold must be determined to remove noise caused by, e.g., Brownian motion and vibrations of the system. The threshold has to be removed from the calculated speed (gray values) for every pixel. We usually use a threshold of 100 nm min^{-1} . The following script performs all of these calculations in Fiji software and measures the total mean speed as gray value:

```
run("Multiply...", "value = 2");  
setThreshold(100, 500000);  
wait(100);  
run("Create Selection");  
run("Measure");
```

If the mean gray value is not shown, it has to be activated in the following submenu: Analyze → Set Measurements → Mean gray value.

3. Prepare histograms by importing the measurements into GraphPad Prism (GraphPad Software).
4. The image displayed at the end of step 2 shows a heat map of mean keratin movement.
5. Note that the saved image still includes the background, which can be permanently removed (submenu: Process → Math → Min).
6. The differences in keratin movement can be visualized by addition of a color LUT (submenu: Image → Lookup Tables). For presentation of the heat maps, the removed gray values have to be considered in the lettering of the color scale.
7. Heat maps of keratin movement from multiple recordings of different cells can be overlaid and averaged (submenu: Image → Stacks → Z-Project → Average Intensity).

The motion analysis process is illustrated in Fig. 3. Figure 4A shows the averaged results for multiple recordings as both heat maps and histograms. A comparison of nonnormalized versus normalized image data highlights similarities in the overall pattern, i.e., no net movement in the cell center and peaks of keratin motility in a ring-shaped domain of the peripheral cytoplasm.

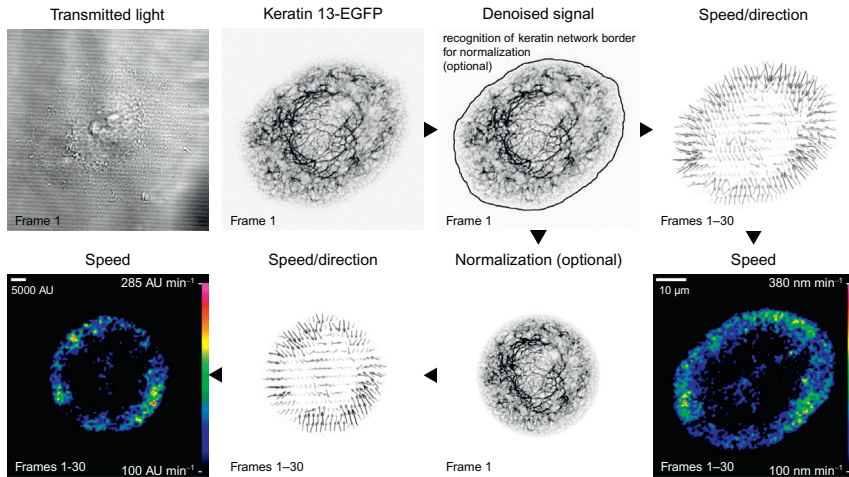


Figure 3 Calculation of keratin speed from time-lapse recordings. The pictures show steps of recording and analyzing keratin motion in a single AK13-1 cell. AK13-1 cells producing keratin 13-EGFP were plated on a laminin 332-rich matrix for 52 h prior to imaging. Phase contrast (transmitted light) and keratin 13-EGFP fluorescence (inverse presentation) were recorded for 15 min every 30 s in the bottom plane. The background was reduced by Anscombe curvelet transform-based denoising (cf. Moch et al., 2013). Optionally, the overall keratin network shape was automatically delineated (black outline) for normalization into a standard circular shape with a defined diameter. A comparison of the non-normalized and the normalized recordings is shown in Movie 3 (<http://dx.doi.org/10.1016/bs.mie.2015.07.034>). The results from motion analysis were then used to prepare vector maps to depict the direction of the movement (corresponding to direction of arrows, which is mostly toward the cell interior). The vectors furthermore show the speed of keratin movement, which corresponds to length and thickness of the vectors. In addition, the speed is shown in detail in heat maps by a color scale as indicated in the images (the speed values correspond to mean speed per pixel).

2.8 Keratin Bulk Flow Analysis

During interphase, the keratin network is continuously moving from the cell periphery toward the cell interior. But this movement does not lead to noticeable keratin accumulation in the cell center because keratin filaments are disassembled into soluble subunits (sinks) that are reused for filament formation in the cell periphery (sources). The resulting keratin bulk flow can be measured from time-lapse recordings of fluorescently tagged keratins with the open source software KeraDyn (Moch et al., 2013). The software determines keratin filament mass from fluorescence intensity (see Protocol 2.7). The algorithm only measures the assembly and disassembly of moving keratin filaments, because nonmotile keratins are not registered by KeraMove:

1. Run the open source software KeraDyn (http://www.moca.rwth-aachen.de/pubs/2013_01/softwarepackage_KeraMove_KeraDyn.zip). The

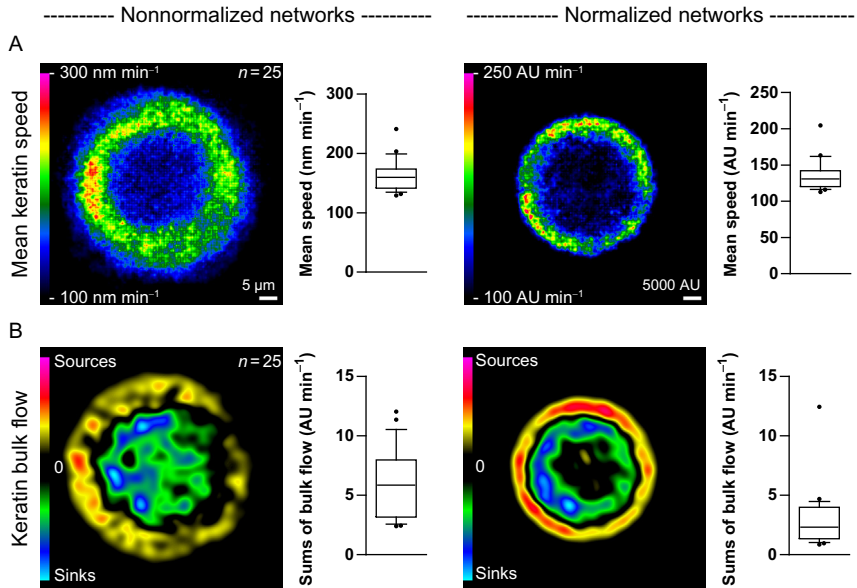
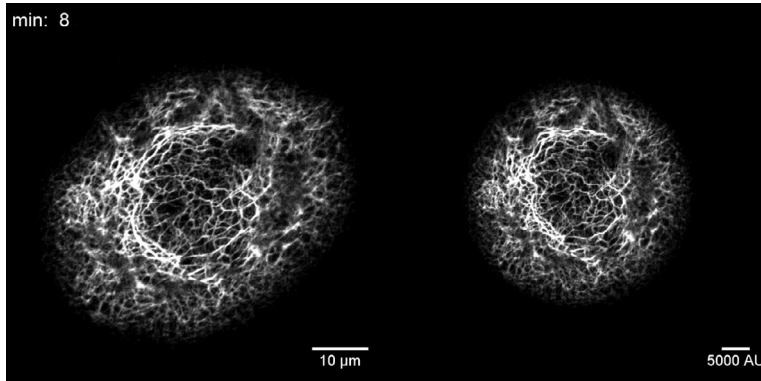


Figure 4 Quantitative measurement of keratin speed (A) and bulk flow (B) in non-normalized and normalized fluorescence recordings of AK13-1 cells expressing keratin 13-EGFP. Fluorescence was recorded in the bottom plane of the cells by confocal microscopy at 30 s intervals for 15 min. The data show the compiled results of standardized measurements of 25 single cell recordings. They are presented as heat maps with subcellular resolution and as whisker box plots (10–90% percentiles). In (A), the heat maps reveal that keratins move faster in the cell periphery than in the cell center underneath the nucleus. The diagrams show that keratin filaments are moving with a median speed of 160 nm min^{-1} before normalization and with 131 AU min^{-1} after normalization of the network shape. In (B), the heat maps show that keratin filaments are primarily assembled in the cell periphery and disassembled in the perinuclear area. Between these two zones keratin is transported and no net keratin assembly or disassembly is detected. The keratin bulk flow can also be described in diagrams as shown in AU. Note that the AU results in diagrams are only of value when different populations/conditions are compared with each other or when data distribution is of interest (e.g., Gaussian distribution).

software generates a map with keratin bulk flow per pixel from analyzed time-lapse recordings of keratin motion (output file: mean_turnover.raw).

2. Import the output file into Fiji software as a heat map in the same way as described for keratin motion maps (see Protocol 2.7). Positive gray values correspond to keratin assembly and negative gray values to keratin disassembly in arbitrary units (AU).
3. For calculation of keratin bulk flow, it is sufficient to measure only the keratin assembly, because sources and sinks balance each other at equilibrium. Therefore, positive gray values are determined by setting the



Movie 3 Denoised recordings of an AK13-1 cell expressing keratin 13-EGFP in a non-normalized (left) and normalized (right) format (corresponding Fig. 3). Note that normalization leads to occasional jumps because of extension/shrinkage of the overall network (time points 13 and 14 min).

threshold to zero. In this way, values equal to zero or smaller are not measured. The following script performs all of these calculations in Fiji software and measures the total bulk flow as integrated densitometry:

```
setThreshold(0.0000000, 1000000000000);
run("NaN Background");
wait(100);
run("Measure");
```

If the integrated densitometry is not shown, it has to be activated in the following submenu: Analyze → Set Measurements → Integrated density.

4. The heat maps of keratin bulk flow can be presented in the same way as described for keratin motion (see Protocol 2.7). Do not remove the background, because only sources would be displayed.
5. Heat maps of keratin bulk flow from multiple recordings of different cells can be overlaid and averaged (submenu: Image → Stacks → Z-Project → Average Intensity).

Figure 4B presents the bulk flow analysis of 25 recordings. Sources of keratin filament fluorescence are detected in the cell periphery (pink–yellow), sinks in the perinuclear cytoplasm (green–blue). Both regions are separated by an area without net turnover (black).

2.9 Keratin Turnover Measured by FRAP

Photobleaching is the photochemical destruction of fluorescence capabilities of a fluorophore. Fluorophores in specific cell regions can be bleached with lasers that are especially developed for this purpose or in confocal

microscopy by the scanning laser at higher intensities. A major problem in FRAP experiments is phototoxic cell damage. In addition, care should be taken to apply bleaching intensities that do not induce cell retraction or other morphological changes.

The method described here is optimized for bleaching keratin filaments in single cells that are not connected to other cells. In these cells, half of the keratin network area is partially bleached which leads to a decrease in total fluorescence. It is important that the bleached network-half has similar organization and brightness ($\pm 10\%$) in comparison to the unbleached part. This will mostly be the case when the keratin cage surrounding the nucleus is localized in the cell center:

1. Choose a cell that fits in a $67 \mu\text{m} \times 67 \mu\text{m}$ area and bleach half of the cell by repeated scanning with 100% laser power for 10 s. It is not necessary to bleach at maximum efficiency. 10–50% is sufficient. It is important, however, to be able to detect the bleached region reliably to account for cell shape changes during the fluorescence recovery time. It is also not necessary to bleach every sample with the same efficiency.
2. Fluorescence transfer from the unbleached to the bleached part is recorded at 0.2% laser intensity in three dimensions at 512×512 pixel (≈ 30 s per projection of complete cell). The chosen scanning speed (image quality) should be sufficient to distinguish the border between the unbleached and bleached regions. The recording of fluorescence recovery should be started directly after bleaching. The fluorescence transfer is recorded for 25 min at time intervals of 5 min.
3. The fluorescence recovery is calculated as the percentage of fluorescence flux from the unbleached to the bleached network part. The ideal choice for control is the unbleached half of the keratin network. The z-stacks from every time interval are opened in Fiji software, and 32-bit sum projections are generated. The background is measured by integrated densitometry at four arbitrary locations of $9.82 \mu\text{m} \times 9.82 \mu\text{m}$ for every time point outside of the cell. It is averaged per pixel and subtracted from the corresponding sum projection.
4. The bleached and unbleached cell halves are outlined by hand with Polygon selections tool for every time point, and corresponding sums of gray values are measured as integrated densitometry. When necessary the regions are corrected at other time points.
5. The fluorescence in the bleached area is defined as $I_{t=n}^b$, and in the unbleached control area as $I_{t=n}^u$ (I = fluorescence intensity, t =time point). For calculation of keratin turnover, $I_{t=0}^b$ is subtracted from $I_{t=n}^b$

and $I_{t=n}^u$ for every time point, and the resulting difference corresponds to the keratin flux from the bleached to unbleached part. For example, at time point zero after bleaching the fluorescence in the unbleached part will always be 100% and in the bleached part 0%.

Figure 5 presents the results of FRAP experiments using the parameters described above.

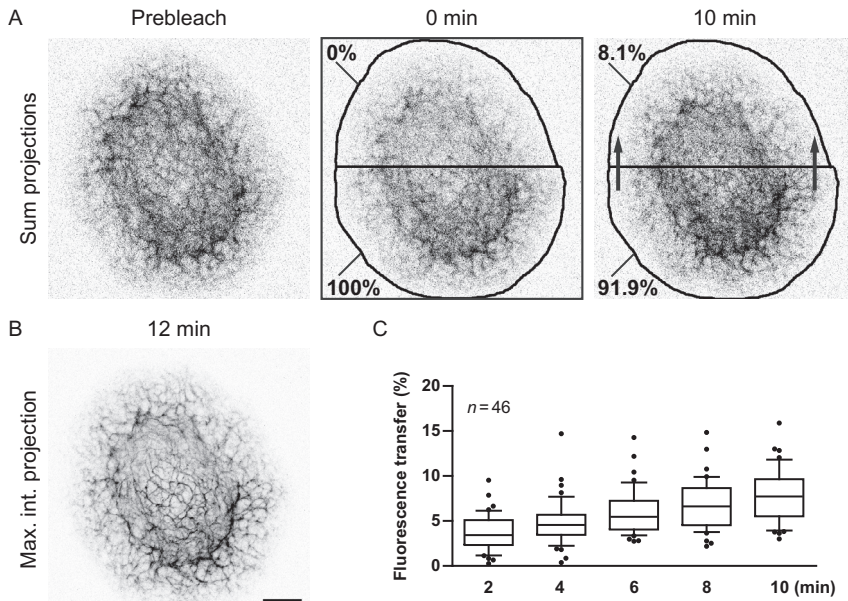
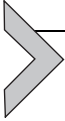


Figure 5 Keratin turnover in cells measured by FRAP. The cells were cultivated for 48–57 h on a laminin 332-rich matrix in the absence of FCS. (A) The fluorescence recordings (inverse presentation of sum projections) of a keratin 13-EGFP-expressing AK13-1 cell. The images depict the fluorescence prior to bleaching (prebleach), immediately after bleaching (0 min), and at the end of a subsequent recording period at 30 s intervals (10 min). To determine the transfer of fluorescence from the unbleached to the bleached part of the cell (arrows), the average fluorescence intensity per pixel was separately calculated for both parts. Next, the fluorescence intensity in the bleached part of the cell was set as 0% at time point 0 min. This value was subtracted from the fluorescence intensity in the unbleached part of the cell, and the resulting fluorescence intensity was defined as 100%. After 10 min, 8.1% of the initial fluorescence in the lower part had been translocated to the upper part. (B) A high-resolution scan as a maximum intensity projection (max. int. projection) of the cell in (A). Note that the border between the bleached and unbleached cell halves is still well demarcated. (C) A histogram of the results of fluorescence transfer measurements as exemplified in (A). The measurements were done in 46 single cells, and the results are shown for time points 2, 4, 6, 8, and 10 min postbleach. The whiskers are 10–90% percentiles. Scale bar: 10 μm .



3. 3D IMAGING OF KERATIN INTERMEDIATE FILAMENTS IN MURINE PREIMPLANTATION EMBRYOS

In the recently described mouse model, which carries a knock-in allele coding for a fluorescently tagged keratin 8 (Krt8-YFP), monitoring the *de novo* synthesis and dynamics of the keratin intermediate filament network has become possible in a physiological 3D context (Schwarz et al., 2015). The type II keratins 8 and 7 are the first intermediate filament proteins expressed in developing murine embryos as early as 2.5 days post conception (dpc) prior to the onset of keratin type I production (Jackson et al., 1980; Lu, Hesse, Peters, & Magin, 2005; Oshima, Howe, Klier, Adamson, & Shevinsky, 1983). Imaging of embryos thus allows following the events that eventually lead to a fully formed keratin intermediate filament network in the trophoctodermal layer.

3.1 Embryo Collection and Cultivation

1. Breed homozygous Krt8-YFP mice naturally and sacrifice plugged female mice at 2.5 dpc by cervical dislocation according to national guidelines for use of laboratory animals.
2. Open the abdominal cavity and push the intestine to one side. Locate the uterus and grasp it with fine forceps. Gently pull the uterus, oviduct, and ovary away from the body cavity (Fig. 6A). Using forceps remove the mesometrium, which is now exposed (Fig. 6B). Locate the oviduct and ovary and grasp the uterus next to the oviduct (Fig. 6C). Gently slide scissors between the oviduct and ovary (do not cut) until they part. Doing so will make flushing easier as the infundibulum will be preserved. Cut next to the forceps, leaving at least 0.5 cm of the uterus and put the oviduct into a culture dish with PBS (D8537, Sigma-Aldrich). Repeat on the other side.
3. Prepare a needle (BD Microlance™ 3 Hypodermic Needle 30G × 1/2", 304000, Becton-Dickinson) by blunting it with sandpaper (Grade: A400) in order to avoid puncturing the oviduct. Fill the syringe (BD Plastipak™ U-40, 300026, Becton-Dickinson) with M2 medium (M7167, Sigma-Aldrich) and make sure that it is free of air bubbles. Place the oviduct on the dry lid of the culture dish under a stereomicroscope and locate the infundibulum (Fig. 6D). Insert the needle and hold it in place with forceps (Fig. 6E). Gently flush the oviduct with ≈ 0.2 ml M2 medium.

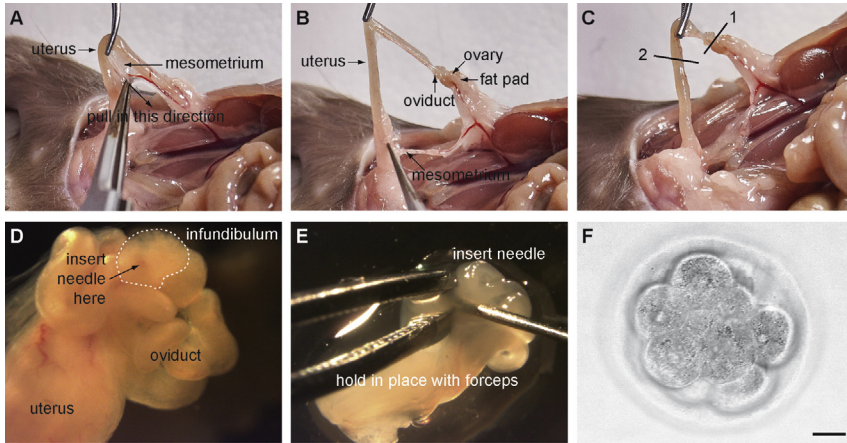


Figure 6 Critical steps of the isolation of preimplantation embryos. After opening the peritoneal cavity, the uterus is held with forceps to pull the mesometrium away (A) and to remove it as well as possible with forceps for exposure of the oviduct and ovary (B). Oviduct and ovary are separated (1 in C), and the uterus is cut as shown (2 in C). The infundibulum of the oviduct is located (D), and a blunted needle is inserted while it is held in place with forceps (E). (F) A healthy looking eight-cell embryo that is ready for further investigation. Scale bar: 20 μm .

4. At 2.5 dpc, eight-cell stage embryos are expected (Fig. 6F). Blastomeres of morphologically healthy looking embryos are round, similar in size, and fill the surrounding zona pellucida. No debris of dissolved cells should be visible. Pick up embryos using a mouth pipette system (embryo handling pipette, 441282, Reproline medical) and wash them through several drops of M2 medium to remove debris. Prepare a microdrop culture dish with 50 μl drops of M16 medium (M7292, Sigma-Aldrich) overlaid with mineral oil (M5310, Sigma-Aldrich). Place embryos individually into microdrops and keep at 37 $^{\circ}\text{C}$ and 5% CO_2 .
5. Let embryos recover for 1 h for studies on the first time appearance of keratin intermediate filaments. From eight-cell stage to blastocyst stage, it will take ≈ 24 h in culture.

3.2 Imaging of Preimplantation Embryos

1. Prewarm the microscope chamber to 37 $^{\circ}\text{C}$.
2. For imaging, prepare a microdrop culture in a glass bottom dish (P35G-0.17-14-C, MatTek) using 50 μl M2 medium overlaid with mineral oil. The mineral oil prevents evaporation of the medium.
3. Transfer a single embryo into the microdrop.

- Record images with a Zeiss LSM 710 Duo microscope. For fluorescence detection, use the 488 nm line of the argon-ion laser and a 63×1.4 N.A. DIC M27 oil immersion objective. Monitor the emitted light between 500 and 590 nm with a pinhole set at 1–2 AU and a laser intensity of 5%. Additionally, record the transmitted light with the T-PMT detector.
- For long-term imaging, the reduction of phototoxicity is of utmost importance. Therefore, intervals between recordings should be as long as possible. We routinely use 15–30 min between imaging of Z-stacks. The embryo can be monitored at a depth of 50 μm without loss in spatial resolution by confocal sectioning (a blastocyst has a diameter of about 100 μm). Therefore, imaging of the whole embryo is not advisable.

A representative recording is presented in Fig. 7 and corresponding Movie 4 (<http://dx.doi.org/10.1016/bs.mie.2015.07.034>). It shows the appearance of diffuse Krt8-YFP fluorescence at the late morula stage with small aggregates appearing upon compaction. In addition, a later stage of keratin network formation is shown in a blastocyst (Fig. 8).

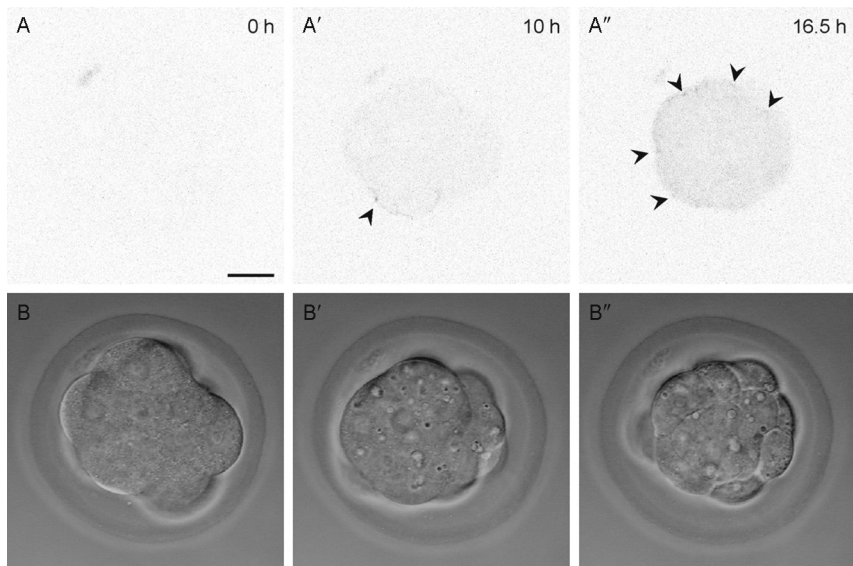
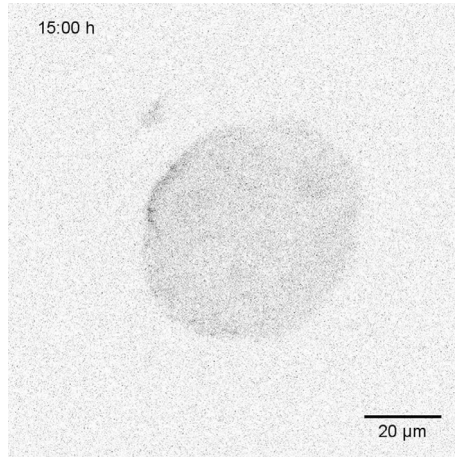


Figure 7 Selected images from a time-lapse recording (Movie 4) of the Krt8-YFP fluorescence (A) and phase contrast optics (B) of a compacting morula. At the beginning, no Krt8-YFP signal is observed. Within 8–10 h, diffuse fluorescence and small fluorescent dots appear (arrow in A'), which increase over time (arrows in A''). Scale bar: 20 μm .



Movie 4 Time-lapse fluorescence recording of a compacted Krt8-YFP embryo shows the first appearance of keratins 10 h after compaction (corresponding [Fig. 7](#)).

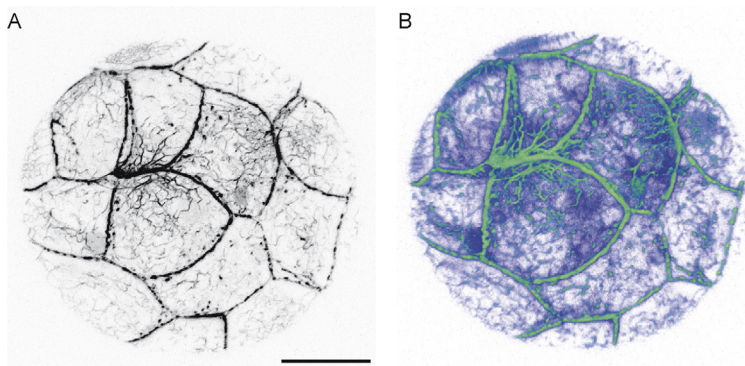


Figure 8 Detection of Krt8-YFP in a late blastocyst by confocal fluorescence microscopy. The maximum intensity projection (A) and 3D reconstruction (B) of the recorded fluorescence (25 focal planes, 1 μm steps) show an extensive network throughout the trophoctoderm layer. Relative fluorescence intensity in (B) is color coded with light green being the strongest and deep blue being the weakest signal. An animation of the reconstruction is presented in [Movie 5](#). Scale bar: 20 μm .

3.3 Image Processing and Analysis

We usually visualize keratin intermediate filament networks in murine pre-implantation embryos either by maximum intensity projection or by 3D reconstruction.

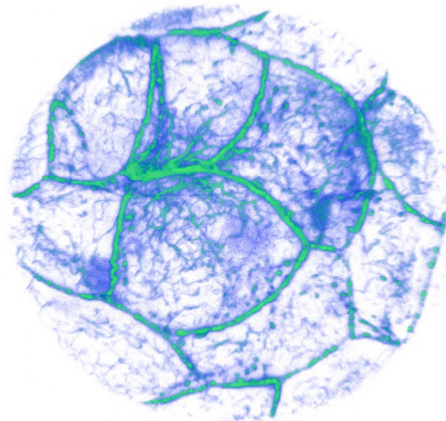
Maximum intensity projection using Fiji software:

1. Run Fiji software (freely available at <http://fiji.sc/Fiji>).
2. Import data into Fiji (Submenu: File → Open).
3. Split channels, if bright-field image is included in data file (Submenu: Image → Color → Split channels).
4. Perform Z-projection for fluorescence channel data (Submenu: Image → Stacks → Z-Project (projection type: max intensity)).
5. If you want to show inverse fluorescence micrographs, choose a gray LUT (Submenu: Image → Lookup Table → Grays) and invert the gray values (Submenu: Image → Lookup Table → Invert LUT).

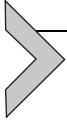
3D reconstruction using Amira software

1. Run Amira software (version 5.5.0, FEI).
2. Open data and load the fluorescence channel in the following submenu.
3. Highlight dataset in Pool window and choose “volren.”
4. Set the following properties in Properties window: color: Volrengreen 1000–50,000; mode: VRT; Shading: none.
5. Create a TIFF file by clicking snapshot and choose tif format.
6. Save file.

Figure 8 shows a projection view and a colored 3D reconstruction (corresponding Movie 5 (<http://dx.doi.org/10.1016/bs.mie.2015.07.034>)) of the keratin network in a late blastocyst.



Movie 5 Animation of a 3D reconstruction of a Krt8-YFP blastocyst (corresponding Fig. 8).



4. OUTLOOK

With the given tools at hand, quantitative assessment of factors influencing keratin intermediate filament network dynamics is now achievable. This will help to understand the complexity of keratin network regulation, its impact on the keratin cycle, and the underlying mechanisms, i.e., signaling pathways, mechanics, and local activity of kinases and phosphatases. By averaging and compiling data of many cells, even subtle alterations become visible. The computational methods presented here can be used to study the dynamics of other intermediate filament networks with some restrictions. The filaments that are formed need to have a certain size and form in order to be ignored by the denoising algorithm (e.g., small round aggregates are filtered out). Furthermore, the algorithms are optimized for particles that are moving rather slowly ($100\text{--}1000\text{ nm min}^{-1}$). For filaments that are moving faster either the recording speed has to be increased in order to apply motion analysis or the code has to be adjusted to detect moving structures over longer distances. It remains to be shown whether the algorithm for bulk flow analysis is applicable for other systems that show a similar behavior.

The Krt8-YFP knock-in mouse line allows tracking of intermediate filament network formation and dynamics and its spatiotemporal determinants in a physiological 3D context. The murine preimplantation embryo is easy to handle and manipulate, and *in vivo* responses of the intermediate filaments to chemical and physical impacts can be faithfully monitored. It is necessary to experimentally test whether the generation of knock-in alleles coding for other intermediate filament - fluorescent protein chimeras is tolerable for the animal and does not cause any perturbations in network structure or function.

Further developments in standardization (e.g., printing procedures), image analysis (e.g., advanced modeling for simulation of network dynamics), monitoring and local regulation of enzymatic activities (e.g., Gardiner et al., 2002; Karginov, Ding, Kota, Dokholyan, & Hahn, 2010; Strickland et al., 2012; Regot, Hughey, Bajar, Carrasco, & Covert, 2014), detection of protein-protein interaction (e.g., by Förster resonance energy transfer, bimolecular fluorescence complementation), and 3D resolution (e.g., light sheet microscopy, super-resolution microscopy) will open exciting new possibilities in the analysis of the plasticity and function of the keratin cytoskeleton. This will help to understand the contribution of the keratin system to epithelial-mesenchymal transition during carcinogenesis and its dysfunction in skin disease.

ACKNOWLEDGMENTS

The work was supported by the German Research Council (LE 566/18, LE 566/20, WI 1731/6, and WI 1731/8).

REFERENCES

- Baribault, H., Blouin, R., Bourgon, L., & Marceau, N. (1989). Epidermal growth factor-induced selective phosphorylation of cultured rat hepatocyte 55-kD cyokeratin before filament reorganization and DNA synthesis. *The Journal of Cell Biology*, *109*, 1665–1676.
- Beriault, D. R., Haddad, O., McCuaig, J. V., Robinson, Z. J., Russell, D., Lane, E. B., et al. (2012). The mechanical behavior of mutant K14-R125P keratin bundles and networks in NEB-1 keratinocytes. *PLoS One*, *7*, e31320.
- Chalfie, M., Tu, Y., Euskirchen, G., Ward, W. W., & Prasher, D. C. (1994). Green fluorescent protein as a marker for gene expression. *Science*, *263*, 802–805.
- Chung, B.-M., Murray, C. I., Eyk, J. E. V., & Coulombe, P. A. (2012). Identification of novel interaction between annexin A2 and keratin 17 evidence for reciprocal regulation. *The Journal of Biological Chemistry*, *287*, 7573–7581.
- Cubitt, A. B., Heim, R., Adams, S. R., Boyd, A. E., Gross, L. A., & Tsien, R. Y. (1995). Understanding, improving and using green fluorescent proteins. *Trends in Biochemical Sciences*, *20*, 448–455.
- Fois, G., Weimer, M., Busch, T., Felder, E. T., Oswald, F., von Wichert, G., et al. (2013). Effects of keratin phosphorylation on the mechanical properties of keratin filaments in living cells. *The FASEB Journal*, *27*, 1322–1329.
- Franke, W. W., Schmid, E., Grund, C., & Geiger, B. (1982). Intermediate filament proteins in nonfilamentous structures: Transient disintegration and inclusion of subunit proteins in granular aggregates. *Cell*, *30*, 103–113.
- Gardiner, E. M., Pestonjamas, K. N., Bohl, B. P., Chamberlain, C., Hahn, K. M., & Bokoch, G. M. (2002). Spatial and temporal analysis of Rac activation during live neutrophil chemotaxis. *Current Biology*, *12*, 2029–2034.
- Ho, C. L., Martys, J. L., Mikhailov, A., Gundersen, G. G., & Liem, R. K. (1998). Novel features of intermediate filament dynamics revealed by green fluorescent protein chimeras. *Journal of Cell Science*, *111*, 1767–1778.
- Jackson, B. W., Grund, C., Schmid, E., Bürki, K., Franke, W. W., & Illmensee, K. (1980). Formation of cytoskeletal elements during mouse embryogenesis. *Differentiation*, *17*, 161–179.
- Karginov, A. V., Ding, F., Kota, P., Dokholyan, N. V., & Hahn, K. M. (2010). Engineered allosteric activation of kinases in living cells. *Nature Biotechnology*, *28*, 743–747.
- Keski-Oja, J., Lehto, V. P., & Virtanen, I. (1981). Keratin filaments of mouse epithelial cells are rapidly affected by epidermal growth factor. *The Journal of Cell Biology*, *90*, 537–541.
- Kölsch, A., Windoffer, R., Würflinger, T., Aach, T., & Leube, R. E. (2010). The keratin-filament cycle of assembly and disassembly. *Journal of Cell Science*, *123*, 2266–2272.
- Ku, N. O., & Omary, M. B. (1997). Phosphorylation of human keratin 8 in vivo at conserved head domain serine 23 and at epidermal growth factor-stimulated tail domain serine 431. *The Journal of Biological Chemistry*, *272*, 7556–7564.
- Lane, E. B., Goodman, S. L., & Trejdosiewicz, L. K. (1982). Disruption of the keratin filament network during epithelial cell division. *The EMBO Journal*, *1*, 1365–1372.
- Langhofer, M., Hopkinson, S. B., & Jones, J. C. (1993). The matrix secreted by 804G cells contains laminin-related components that participate in hemidesmosome assembly in vitro. *Journal of Cell Science*, *105*, 753–764.
- Leube, R. E., Moch, M., Kölsch, A., & Windoffer, R. (2011). Panta rhei. *BioArchitecture*, *1*, 39–44.
- Leube, R. E., Moch, M., & Windoffer, R. (2015). Intermediate filaments and the regulation of focal adhesion. *Current Opinion in Cell Biology*, *32*, 13–20.

- Liovic, M., Mogensen, M. M., Prescott, A. R., & Lane, E. B. (2003). Observation of keratin particles showing fast bidirectional movement colocalized with microtubules. *Journal of Cell Science*, *116*, 1417–1427.
- Lu, H., Hesse, M., Peters, B., & Magin, T. M. (2005). Type II keratins precede type I keratins during early embryonic development. *European Journal of Cell Biology*, *84*, 709–718.
- Mittal, B., Sanger, J. M., & Sanger, J. W. (1989). Visualization of intermediate filaments in living cells using fluorescently labeled desmin. *Cell Motility and the Cytoskeleton*, *12*, 127–138.
- Moch, M., Herberich, G., Aach, T., Leube, R. E., & Windoffer, R. (2013). Measuring the regulation of keratin filament network dynamics. *Proceedings of the National Academy of Sciences of the United States of America*, *110*, 10664–10669.
- Okabe, S., Miyasaka, H., & Hirokawa, N. (1993). Dynamics of the neuronal intermediate filaments. *The Journal of Cell Biology*, *121*, 375–386.
- Oshima, R. G., Howe, W. E., Klier, F. G., Adamson, E. D., & Shevinsky, L. H. (1983). Intermediate filament protein synthesis in preimplantation murine embryos. *Developmental Biology*, *99*, 447–455.
- Prahlad, V., Yoon, M., Moir, R. D., Vale, R. D., & Goldman, R. D. (1998). Rapid movements of vimentin on microtubule tracks: Kinesin-dependent assembly of intermediate filament networks. *The Journal of Cell Biology*, *143*, 159–170.
- Regot, S., Hughey, J. J., Bajar, B. T., Carrasco, S., & Covert, M. W. (2014). High-sensitivity measurements of multiple kinase activities in live single cells. *Cell*, *157*, 1724–1734.
- Rolli, C. G., Seufferlein, T., Kemkemer, R., & Spatz, J. P. (2010). Impact of tumor cell cytoskeleton organization on invasiveness and migration: A microchannel-based approach. *PLoS One*, *5*, e8726.
- Schwarz, N., Windoffer, R., Magin, T. M., & Leube, R. E. (2015). Dissection of keratin network formation, turnover and reorganization in living murine embryos. *Scientific Reports*, *5*.
- Strickland, D., Lin, Y., Wagner, E., Hope, C. M., Zayner, J., Antoniou, C., et al. (2012). TULIPs: Tunable, light-controlled interacting protein tags for cell biology. *Nature Methods*, *9*, 379–384.
- Strnad, P., Windoffer, R., & Leube, R. E. (2003). Light-induced resistance of the keratin network to the filament-disrupting tyrosine phosphatase inhibitor orthovanadate. *The Journal of Investigative Dermatology*, *120*, 198–203.
- Vikstrom, K. L., Lim, S. S., Goldman, R. D., & Borisy, G. G. (1992). Steady state dynamics of intermediate filament networks. *The Journal of Cell Biology*, *118*, 121–129.
- Wang, L., Ho, C., Sun, D., Liem, R. K. H., & Brown, A. (2000). Rapid movement of axonal neurofilaments interrupted by prolonged pauses. *Nature Cell Biology*, *2*, 137–141.
- Windoffer, R., Beil, M., Magin, T. M., & Leube, R. E. (2011). Cytoskeleton in motion: The dynamics of keratin intermediate filaments in epithelia. *The Journal of Cell Biology*, *194*, 669–678.
- Windoffer, R., & Leube, R. E. (1999). Detection of cytokeratin dynamics by time-lapse fluorescence microscopy in living cells. *Journal of Cell Science*, *112*, 4521–4534.
- Windoffer, R., & Leube, R. E. (2001). De novo formation of cytokeratin filament networks originates from the cell cortex in A-431 cells. *Cell Motility and the Cytoskeleton*, *50*, 33–44.
- Windoffer, R., & Leube, R. E. (2004). Imaging of keratin dynamics during the cell cycle and in response to phosphatase inhibition. *Methods in Cell Biology*, *78*, 321–352.
- Windoffer, R., Wöll, S., Strnad, P., & Leube, R. E. (2004). Identification of novel principles of keratin filament network turnover in living cells. *Molecular Biology of the Cell*, *15*, 2436–2448.
- Yoon, M., Moir, R. D., Prahlad, V., & Goldman, R. D. (1998). Motile properties of vimentin intermediate filament networks in living cells. *The Journal of Cell Biology*, *143*, 147–157.

- Yoon, K. H., Yoon, M., Moir, R. D., Khuon, S., Flitney, F. W., & Goldman, R. D. (2001). Insights into the dynamic properties of keratin intermediate filaments in living epithelial cells. *The Journal of Cell Biology*, *153*, 503–516.
- Yuan, A., Sasaki, T., Rao, M. V., Kumar, A., Kanumuri, V., Dunlop, D. S., et al. (2009). Neurofilaments form a highly stable stationary cytoskeleton after reaching a critical level in axons. *The Journal of Neuroscience*, *29*, 11316–11329.